Nano Research

Open Access

Research Article

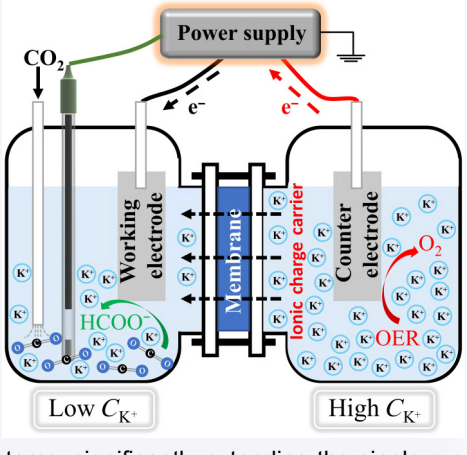
Concentration-gradient strategy for controllable cell voltage in electrocatalytic reduction of CO_2 to high-concentration formate

Jianhe Liu[1,3,§], Liming Yang[1,§], Tao Yang[1,2,3] ✉, Shengbing Dong[1], Shuang Liu[1], Kang Wang[1], Xiangtao Yu[1], Sheng Cao[4], Zhentao Du[4], Shanglin Lv[5] ✉, and Xinmei Hou[1,2,6] ✉

[1] *Institute for Carbon Neutrality, University of Science and Technology Beijing, Beijing 100083, China*
[2] *Institute of Steel Sustainable Technology, Liaoning Academy of Materials, Shenyang 110000, China*
[3] *Key Laboratory of Green Extraction & Efficient Utilization of Light Rare-Earth Resources (Inner Mongolia University of Science and Technology), Ministry of Education, Baotou 014010, China*
[4] *School of Physical Science and Technology, State Key Laboratory of Featured Metal Materials and Life-Cycle Safety for Composite Structures, Guangxi University, Nanning 530004, China*
[5] *Key Laboratory of Quality Inspection and Monitoring of Construction Steel and Products, State Administration for Market Regulation, Central Research Institute of Building and Construction Co., Ltd., MCC, Beijing 100088, China*
[6] *Beijing Advanced Innovation Center for Materials Genome Engineering, University of Science and Technology Beijing, Beijing 100083, China*
§ *Jianhe Liu and Liming Yang contributed equally to this work.*

Cite this article: *Nano Research*, **2026**, *19*, 94908710. https://doi.org/10.26599/NR.2026.94908710

ABSTRACT: In CO_2 electroreduction systems using neutral or alkaline electrolytes with cation exchange membranes, the rising cell voltage during operation increases energy consumption, limits formate accumulation, and compromises long-term stability. In this work, an H-type cell was employed as a model to systematically investigate both neutral $KHCO_3$ and alkaline KOH electrolyte systems. It was elucidated that K^+, acting as the primary charge carriers, continuously migrates from the anode compartment to the cathode compartment. This migration results in the development of a concentration gradient and an associated increase in diffusion potential, ultimately leading to a continuous rise in the overall cell voltage. Based on this understanding, a "concentration-gradient" strategy was proposed, in which the concentration of the anolyte is increased to alleviate the conflict between formate accumulation and rising cell voltage. This strategy effectively limits cell voltage fluctuations within ±0.5 V and enables continuous and stable operation for up to 30 h, approximately 3 to 4 times longer than durations previously reported for conventional 1 mol·L^{-1} $KHCO_3$ systems, significantly extending the single-run operation time. The formate yield reached 310 μmol·cm^{-2}·h^{-1}·mA^{-1}, representing an increase of 200% compared to the average level. In addition, similar results were obtained using $NaHCO_3$ as the electrolyte, demonstrating the broad applicability of this strategy.



KEYWORDS: CO_2, formate, CO_2 reduction reaction (CO_2RR), cell voltage, electrolyte

1 Introduction

The electrochemical CO_2 reduction reaction (CO_2RR) has attracted widespread attention due to its ability to convert greenhouse gases into value-added chemicals under ambient temperature and pressure. Among various reduction products, formate (HCOOH) has emerged as one of the most studied targets because of its simple reaction pathway, liquid-state product form that facilitates storage, and wide range of downstream applications [1–6]. H-type cell and flow cell are currently the most widely studied electrolytic systems for electrocatalytic reduction of CO_2 to formate. Both consist of a cathode chamber, an anode chamber, and an ion exchange membrane. Formate can be obtained by accumulating and

Received: August 12, 2025
Accepted: April 3, 2026

✉Address correspondence to Tao Yang, yangtaoustb@ustb.edu.cn; Shanglin Lv, lvshanglin@126.com; Xinmei Hou, houxinmeiustb@ustb.edu.cn

purifying it from the catholyte. However, the currently achievable concentration is typically limited to around 10–90 mmol·L^{-1}, whereas a concentration exceeding 2.2 mol·L^{-1} is required for economically viable industrial production [7–21]. To suppress the crossover and subsequent oxidation of formate from the cathode to the anode, cation exchange membranes are commonly used as separators. However, such electrolytic cells often exhibit a continuous increase in cell voltage during operation, which leads to higher energy consumption and is unfavorable for continuous industrial production [22]. According to the study by Zheng et al., at a current density of 20 mA·cm^{-2}, the cell voltage increased from approximately −5 to −9 V within just 1.5 h, corresponding to a rise of about 2.7 V per hour [23–26]. To address this issue, researchers have attempted to mitigate the continuous rise in cell voltage by periodically refreshing the electrolyte or increasing its volume. Although these methods can temporarily slow the voltage increase, they significantly dilute the formate product, which fundamentally contradicts the goal of achieving high product concentration [13, 14, 17, 18, 27–43]. For example, Yi et al. increased the electrolyte volume to 1000 mL, resulting in a formate concentration of only 0.06 mmol·L^{-1} [18], far below the average level. Therefore, it is urgently necessary to develop strategies that can simultaneously suppress cell voltage escalation and enhance formate concentration.

Considering that the rise in cell voltage occurs rapidly, within a few to several hours, which is significantly shorter than the lifespans of catalysts (hundreds of hours) and ion-exchange membranes (tens of thousands of hours), it is likely that this increase is caused by changes in the electrolyte [44]. Previous studies have indicated that the types and concentrations of cations and anions in the electrolyte can influence the performance of the catalyst [3, 45–47]. For example, when studying sulfur-doped indium catalysts for the CO_2RR, Ma et al. found that the type of cation in the electrolyte (Na^+, K^+, and Cs^+) significantly influences the formate production rate. Among these cations, Cs^+ enabled a high formate production rate of 1449 μmol·h^{-1}·cm^{-2} while maintaining a Faradaic efficiency (FE) for formate of 93%. In addition, isotope-labeling experiments ($H_2O \rightarrow D_2O$) confirmed that water is continuously activated and participates in product formation during the reaction, indicating that the electrolyte composition dynamically evolves over the course of the reaction [10]. These changes mainly originate from three aspects: (1) the generation of new ions at the electrode/electrolyte interface during the CO_2RR; (2) neutralization reactions between ions in the electrolyte solution; and (3) ion migration through the ion exchange membrane. The combined effects of these factors contribute to the rise in cell voltage. In practical operation, regardless of the type of electrolyte used, changes in electrolyte composition during the CO_2RR are almost universally observed [48]. However, which of these factors plays the dominant role in driving electrolyte changes and the resulting continuous increase in cell voltage has not been systematically investigated.

In this study, a typical H-type cell was employed to systematically investigate the evolution of electrolytes during the electrocatalytic reduction of CO_2 to formate using a proton exchange membrane (PEM) and two commonly used electrolytes: $KHCO_3$ and KOH. It was identified in this work that the continuous increase in cell voltage is caused by the unidirectional migration of K^+ from the anode to the cathode. Building on this foundation, a "concentration-gradient" strategy was proposed that effectively suppresses the continuous rise in cell voltage, maintaining voltage fluctuations within ±0.5 V. Within this stable range, the catalyst achieved over 30 h of uninterrupted operation per run, which is 3–4 times longer than the durations reported in previous studies. Using $KHCO_3$ as the electrolyte, a single run yielded a formate concentration of 50.6 mg·L^{-1}, with a normalized productivity reaching approximately 310 μmol·cm^{-2}·h^{-1}·mA^{-1}, increasing to 200% of the average level.

2 Material and methods

2.1 Chemicals and materials

All chemicals used in this work were of analytical grade and used without further treatments. Anhydrous ethanol, bismuth nitrate pentahydrate ($Bi(NO_3)_3$·$5H_2O$), potassium bicarbonate ($KHCO_3$), and sodium sulphate (Na_2SO_4) were purchased from Macklin, and deionized water was obtained from a Millipore system. Hydrochloric acid was purchased from Sinopharm Chemical Reagent Co., Ltd., hydrophobic carbon cloth (HCP331P) was purchased from Toray Industries, Nafion membranes (N117) were provided by Gaoss Union, and carbon dioxide gas (99.999% purity) was provided by Beijing Haipu Gas Co., Ltd.

2.2 Synthesis of the Bi catalyst

Hydrophobic carbon cloth was employed as the substrate to grow Bi, which was pretreated by consecutive ultrasonication in deionized water and anhydrous ethanol. The catalyst precursor was prepared using 0.2 mol·L^{-1} bismuth nitrate pentahydrate (4.85 g), 5 mL of concentrated hydrochloric acid, and 45 mL of deionized water. A two-electrode electrochemical system was used for electrodeposition in this work, with several pretreated hydrophobic carbon cloth serving as the working electrode and platinum foil as the counter electrode. The electrodeposition was optimized to constant current electrodeposition at −15 mA·cm^{-2} for 20 min. After the electrodeposition process, the obtained Bi on hydrophobic carbon cloth was rinsed repeatedly with deionized water and ethanol, and then dried at room temperature overnight.

2.3 Electrochemical measurements

30 mL of H-type cell equipped with a PEM was used as the reaction system (Fig. S1 in the Electronic Supplementary Material (ESM)). Two representative electrolytes, $KHCO_3$ and KOH, were employed for comparative investigation. All experiments were conducted using a self-fabricated bismuth-based catalyst as the working electrode (Figs. S2–S4 in the ESM), a commercial platinum foil as the counter electrode, and an Ag/AgCl electrode as the reference electrode. All electrode potentials were converted to values relative to the reversible hydrogen electrode (vs. RHE) using the calculation equation: $E_{(vs.RHE)} = E_{(vs.Ag/AgCl)} + 0.1976\ V + 0.0591 \times pH$. Electrochemical measurements were carried out using a Corrtest CS2350M potentiostat under the following conditions: a constant gas flow rate of 5 sccm, a constant current density of 50 mA·cm^{-2} (with an effective geometric area of 1 cm × 1 cm), and 25 mL of electrolyte solution in both the cathode and anode compartments.

First, 1 mol·L^{-1} $KHCO_3$ and KOH were selected as the electrolytes. Samples were collected from both the cathode and anode chambers at 0, 3.5, 7, and 10.5 h to measure the concentrations of K^+ and HCO_3^-, as well as the pH and conductivity.

Subsequently, for both $KHCO_3$ and KOH electrolytes, four concentration gradients were set: 0.5, 1, 1.5, and 2 mol·L^{-1}. The CO_2RR performance under different concentrations was

systematically investigated, with particular focus on the time required for the cell voltage to drop from its initial value to −10 V. During the electrolysis process, 100 μL of catholyte was sampled every 2 h and analyzed for formate concentration using ion chromatography.

Finally, a concentration-gradient strategy was employed, in which a low-concentration electrolyte solution (0.5 mol·L^{-1}) was used in the cathode chamber and a saturated $KHCO_3$ electrolyte solution (3.37 mol·L^{-1}) was used in the anode chamber. Using the controlled variable experimental method, in the KOH electrolyte solution experiment, the concentration of the anode electrolyte solution was also 3.37 M (Fig. S7 in the ESM). During electrolysis, catholyte samples were collected every 2 h to measure the FE for formate. To systematically compare the effectiveness of this strategy, two control experiments were conducted: (1) Both cathode and anode chambers were filled with 1 mol·L^{-1} $KHCO_3$ or KOH solution, and the anolyte was refreshed each time the cell voltage increased by 1 V, allowing the reaction to continue. (2) Both chambers contained 1 mol·L^{-1} electrolyte, and both the catholyte and anolyte were refreshed simultaneously when the cell voltage rose by 1 V. Additionally, the universality of the "concentration-gradient" strategy was verified using $NaHCO_3$ as the electrolyte.

2.4 Characterization

The pH and conductivity of the solution were measured using a Leizhi PHS-25 pH meter and a DDS-307 conductivity meter, respectively. The concentrations of K^+ and HCO_3^- were determined by inductively coupled plasma optical emission spectrometry (ICP-OES, Thermo Fisher iCAP 7400). Liquid-phase ion analysis was conducted using an EP-1000 ion chromatograph. The surface morphology of the samples was characterized by scanning electron microscopy (SEM, FEI ApreoLoVac). X-ray diffraction (XRD) patterns were obtained using a Bruker D8 Advance diffractometer.

3 Results and discussion

3.1 Electrolyte evolution

3.1.1 $KHCO_3$ electrolyte evolution

As shown in Figs. 1(a) and 1(b), with increasing reaction time, the K^+ concentration in the cathode chamber increased from the initial 0.96 to 1.79 mol·L^{-1}, and the HCO_3^- concentration rose from 0.95 to 1.36 mol·L^{-1}. In contrast, the K^+ concentration in the anode chamber significantly decreased from 0.96 to 0.10 mol·L^{-1}, and the HCO_3^- concentration dropped from 0.95 to 0.08 mol·L^{-1}. As shown in Figs. 1(c) and 1(d), the conductivity of the anolyte continuously decreased from 74.63 to 22.37 μS·cm^{-1}, while the conductivity of the catholyte steadily increased from 71.17 to 115.07 μS·cm^{-1}. Regarding pH, the cathode chamber showed a trend of first decreasing and then increasing. It dropped from 9.15 to 8.47, and then rose to 8.71. Meanwhile, the pH value in the anode chamber continuously decreased from 9.53 to 8.74. The above changes can be attributed to the following mechanisms: When $KHCO_3$ is used as the electrolyte, the initial decrease is primarily driven by the acidification effect from CO_2 saturation and partial proton migration from the anode. However, as the electrolysis continues, CO_2 is reduced at the cathode to form $HCOO^-$ and OH^-. The generated OH^- eventually accumulates and reacts with excess CO_2 in the solution to produce additional HCO_3^-, leading to the dominant alkalization of the catholyte and an increase in pH. At the anode, oxygen evolution reaction (OER) generates H^+, but only a small portion of the H^+ can migrate through the proton exchange membrane to the cathode. Most of the H^+ reacts with HCO_3^- to form H_2O and CO_2. Since the H^+ generated from OER cannot fully migrate to the cathode to maintain charge neutrality, K^+ ions are forced to serve as the primary charge carriers, migrating from the anode to the cathode to preserve electroneutrality in the system [17, 38, 49, 50]. As shown in Fig. 1(e), this process results in a significant decrease in K^+ concentration in the anode chamber, gradually converting the solution into a near-pure water system. Consequently, the conductivity drops sharply, leading to an increase in solution resistance. This creates a pronounced concentration gradient between the cathode and anode chambers, generating a large diffusion potential in the same direction as the cell's electromotive force. This manifests in the cell voltage as a substantial Ohmic drop. As shown in Fig. 1(f), the cell voltage increased from −5.70 to −10 V in less than 12 h. After the electrolyte was refreshed, the cell voltage returned to approximately −6.00 V, indicating that the rise in cell voltage was caused by changes in the electrolyte solution. The cathodic and anodic half-reactions using $KHCO_3$ as the electrolyte are given in Eqs. (1)–(4)

Catholyte:

$$CO_2 + 2e^- + H_2O \rightarrow HCOO^- + OH^- \quad (1)$$

$$CO_2 + OH^- \rightarrow HCO_3^- \quad (2)$$

Anolyte:

$$H_2O \rightarrow \frac{1}{2}O_2 + 2H^+ + 2e^- \quad (3)$$

$$HCO_3^- + H^+ \rightarrow H_2O + CO_2 \quad (4)$$

3.1.2 KOH electrolyte evolution

When the electrolyte was replaced with KOH solution, a similar trend to that observed in the $KHCO_3$ system was found. As shown in Fig. 2(a), the K^+ concentration in the cathode chamber increased from the initial 0.97 to 1.82 mol·L^{-1}, while in the anode chamber it decreased from 0.97 to 0.10 mol·L^{-1}. As shown in Figs. 2(b)–2(d), at the beginning of the reaction, the KOH solution in the cathode chamber had already been largely converted into $KHCO_3$ with a concentration of approximately 0.75 mol·L^{-1}. After 10.5 h of electrolysis, the HCO_3^- concentration further increased to 1.25 mol·L^{-1}, the conductivity rose from 69.87 to 115.13 μS·cm^{-1}, and the pH decreased from 9.50 to 8.48 before rising again to 8.64. As the reaction proceeded, the OH^- concentration in the anode chamber decreased from the initial 0.96 to 0.12 mol·L^{-1}. At 10.5 h into the reaction, the conductivity of the anolyte decreased from the initial value of 228.43 to 34.8 μS·cm^{-1}, while the pH exhibited an overall downward trend, decreasing from 13.97 to 13.67. When KOH is used as the electrolyte, the consumption pathway of CO_2 at the cathode consists of two parts: One portion of CO_2 undergoes a chemical reaction with OH^- to form HCO_3^-, while the other is electrochemically reduced to $HCOO^-$ and OH^-. Prior to the complete conversion of KOH to $KHCO_3$ at the cathode, chemical and electrochemical processes act as competing reactions for CO_2 consumption [51–54]. At the anode, the OER takes place, where OH^- is oxidized to generate O_2 and H_2O. Meanwhile, in accordance

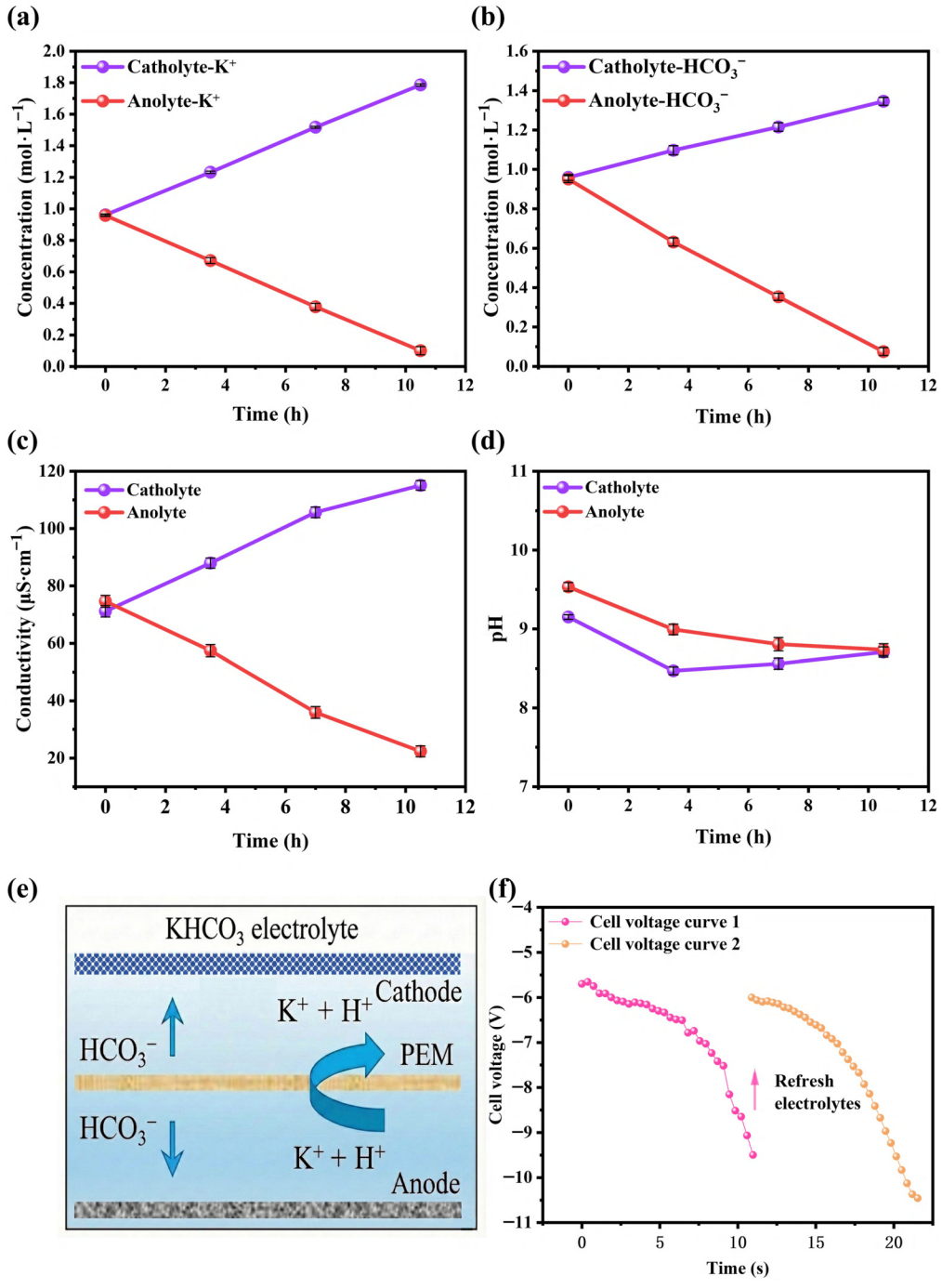


Figure 1 Reaction mechanism of CO_2 reduction using $KHCO_3$ as the electrolyte. ((a) and (b)) Dynamic changes in K^+ and HCO_3^- concentrations in the cathode and anode chambers. ((c) and (d)) Variation trends of conductivity and pH in the cathode and anode chambers. (e) Schematic of the reaction mechanism in an H-type cell using $KHCO_3$ as the electrolyte. (f) Cell voltage.

with the principle of electroneutrality, K^+ is the sole charge carrier migrating across the proton exchange membrane from the anode to the cathode in the KOH electrolyte system, as illustrated in Fig. 2(e). As shown in Fig. 2(f), when the reaction proceeded to 11.6 h, the cell voltage increased to −10 V. After refreshing the electrolyte at that point, the cell voltage returned to its initial value of approximately −4.80 V, further indicating that the voltage rise was caused by changes in the electrolyte solution. The cathodic and anodic half-reactions with KOH as the electrolyte are presented in Eqs. (5)–(7)

Catholyte:

$$CO_2 + 2e^- + H_2O \rightarrow HCOO^- + OH^- \quad (5)$$

$$CO_2 + OH^- \rightarrow HCO_3^- \quad (6)$$

Anolyte:

$$2OH^- \rightarrow \frac{1}{2}O_2 + H_2O + 2e^- \quad (7)$$

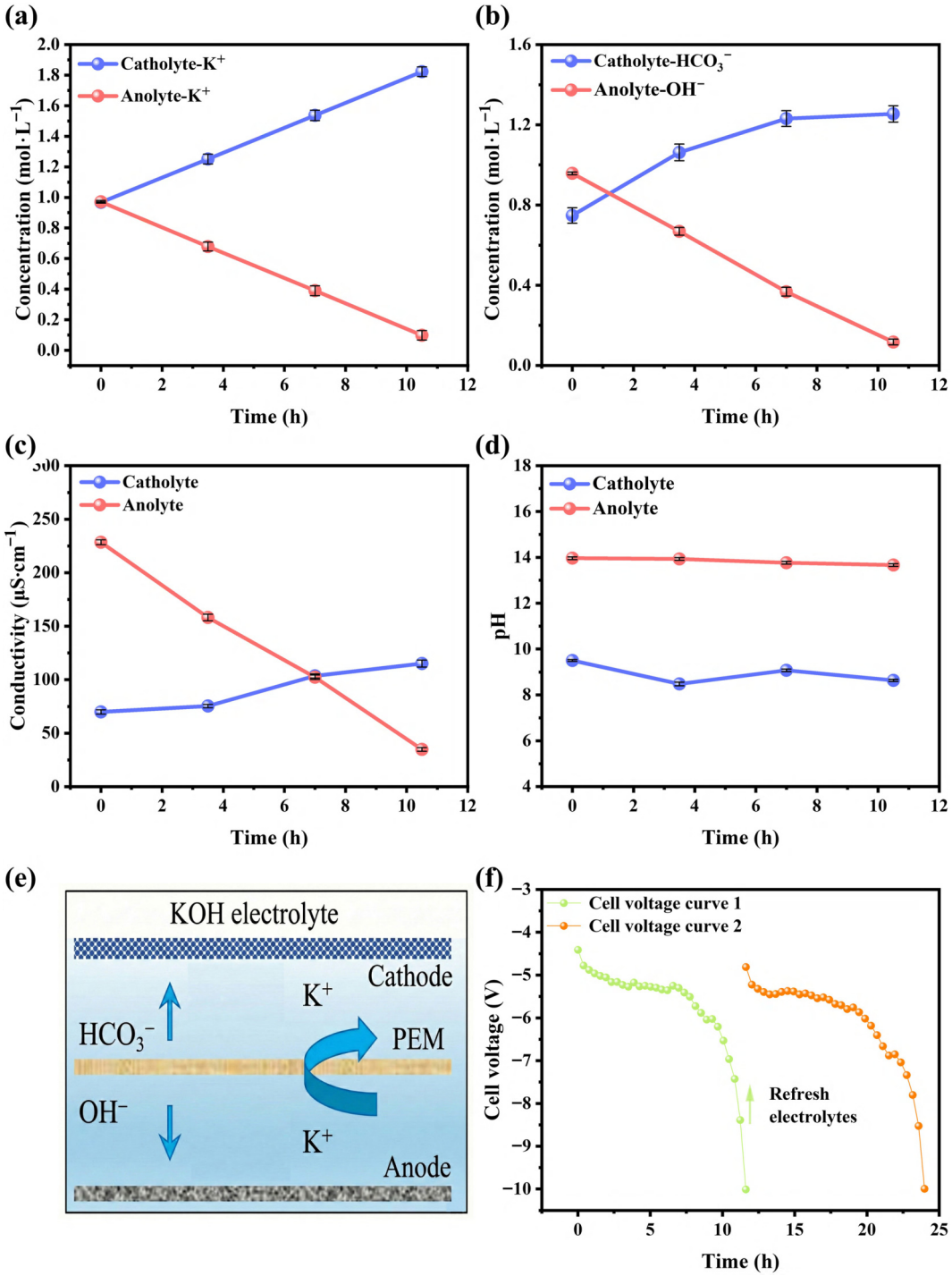


Figure 2 Reaction mechanism of CO_2 reduction using KOH as the electrolyte. ((a) and (b)) Dynamic changes in K^+ and OH^-/HCO_3^- concentrations in the cathode and anode chambers. ((c) and (d)) Variation trends of conductivity and pH in the cathode and anode chambers. (e) Schematic of the reaction mechanism in an H-type cell using KOH as the electrolyte. (f) Cell voltage.

3.2 Effect of electrolyte concentration

3.2.1 Effect of $KHCO_3$ electrolyte concentration

Different electrolyte concentrations imply varying K^+ concentrations, and since K^+ serves as the primary charge carrier, its concentration may significantly affect the initial cell voltage, reaction duration, product concentration, and FE. To systematically evaluate the influence of electrolyte concentration, $KHCO_3$ was selected as the model electrolyte. As shown in Fig. 3(a), increasing the $KHCO_3$ concentration from 0.5 to 2 mol·L^{-1} led to a notable decrease in the initial cell voltage, from approximately −7.23 to −5.43 V. Notably, as shown in Fig. 3(b), the FE for formate remained consistently above 90% regardless of whether high- or low-concentration $KHCO_3$ solutions were used. As shown in Fig. 3(c), the reaction time required for the cell voltage to reach −10 V increased by approximately 5 h for every 0.5 mol·L^{-1} increase

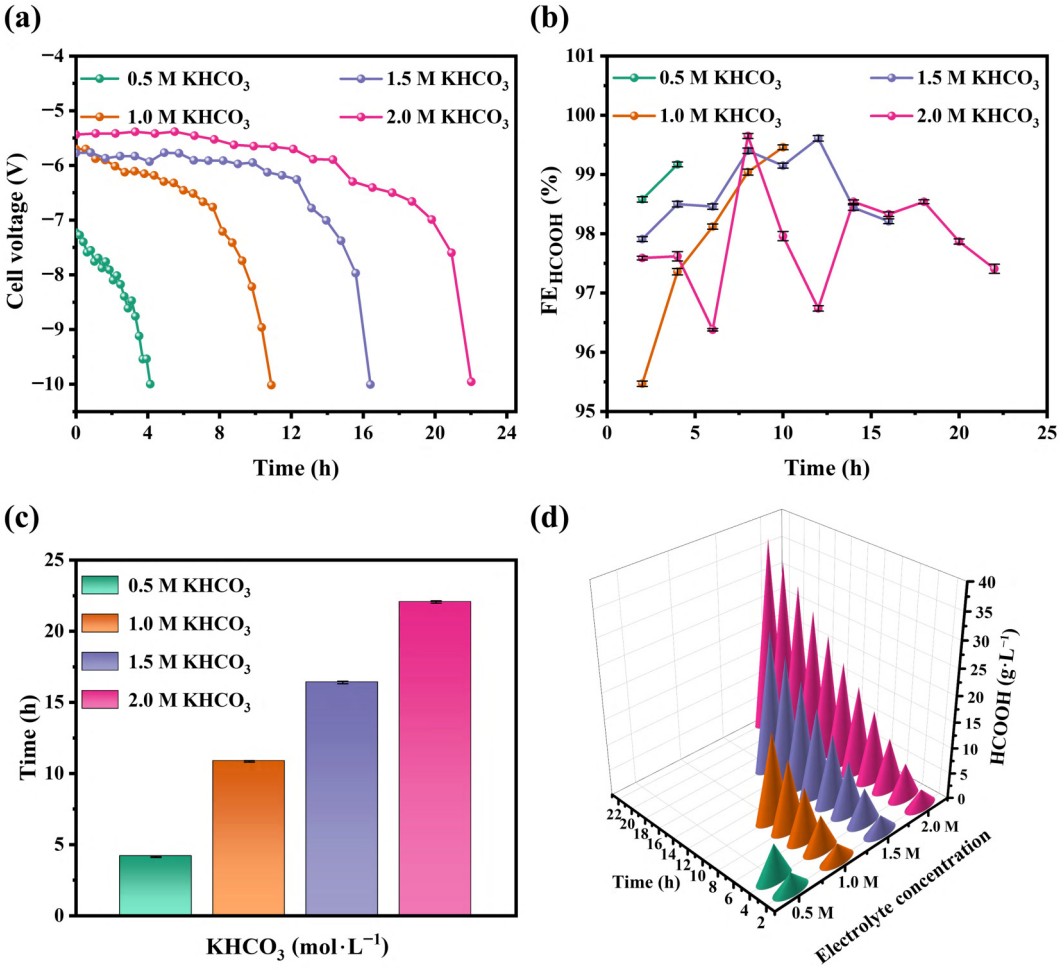


Figure 3 Effects of $KHCO_3$ electrolyte concentration. (a) Variation of cell voltage over time at different $KHCO_3$ concentrations. (b) Influence of $KHCO_3$ concentration on the FE for formate. (c) Time required to reach −10 V during electrolysis at various $KHCO_3$ concentrations. (d) Effect of $KHCO_3$ concentration on formate production.

in electrolyte concentration. Additionally, as illustrated in Fig. 3(d), the accumulated $HCOO^-$ concentration reached 36.8 mg·L^{-1} in 2 mol·L^{-1} $KHCO_3$ solution, indicating that a higher electrolyte concentration not only facilitates greater accumulation of formate but also reduces energy consumption.

3.2.2 Effect of KOH electrolyte concentration

Similarly, four different concentrations of KOH electrolyte were tested to evaluate its performance in electrocatalytic reduction of CO_2 to formate. As shown in Figs. 4(a) and 4(c), increasing the KOH concentration from 0.5 to 2 mol·L^{-1} led to a clear decrease in the initial cell voltage, from approximately −6.0 to −3.7 V. Meanwhile, the reaction time required for the cell voltage to drop to −10 V was extended by about 5 h for every 0.5 mol·L^{-1} increase in KOH concentration, showing a trend similar to that observed in the $KHCO_3$ system. However, it is noteworthy that under the same concentration conditions, the initial cell voltage with KOH electrolyte was consistently lower than that with $KHCO_3$, which is advantageous for reducing energy consumption. As shown in Fig. 4(b), the FE in the KOH system was generally below 90% at the beginning of the reaction, but gradually increased with time and eventually stabilized above 90%. This behavior is attributed to the fact that, during the early stage of the reaction, most of the CO_2 initially undergoes a chemical reaction with OH^- to form HCO_3^-, while only a small fraction of CO_2 is electrochemically reduced to $HCOO^-$. As shown in Fig. 4(d), higher KOH concentrations correspond to higher OH^- concentrations, which increase the proportion of the chemical pathway, thereby suppressing the initial FE for formate production. Only after KOH is sufficiently converted to $KHCO_3$ does CO_2 become more accessible for electrochemical reduction (CO_2RR), resulting in a FE for formate that exceeds 90%.

Therefore, regardless of whether $KHCO_3$ or KOH is used as the electrolyte, increasing the electrolyte concentration can effectively reduce the initial cell voltage, thereby improving energy efficiency. For the $KHCO_3$ system, changes in electrolyte concentration have little impact on formate production, with the FE consistently maintained at a high level. In contrast, in the KOH system, CO_2 preferentially reacts with OH^- during the initial stage to form HCO_3^-, which suppresses the electrochemical reduction of CO_2 and results in a significantly lower initial FE for formate. Moreover, this suppression effect becomes more pronounced at higher KOH concentrations. These results suggest that rational regulation of electrolyte concentration can not only reduce cell voltage but also, to a certain extent, enable more efficient accumulation of formate.

3.3 Concentration-gradient strategy

This study proposes a "concentration-gradient" strategy, in which the anolyte is intentionally set at a higher concentration than the catholyte to generate an ohmic potential drop opposite to the

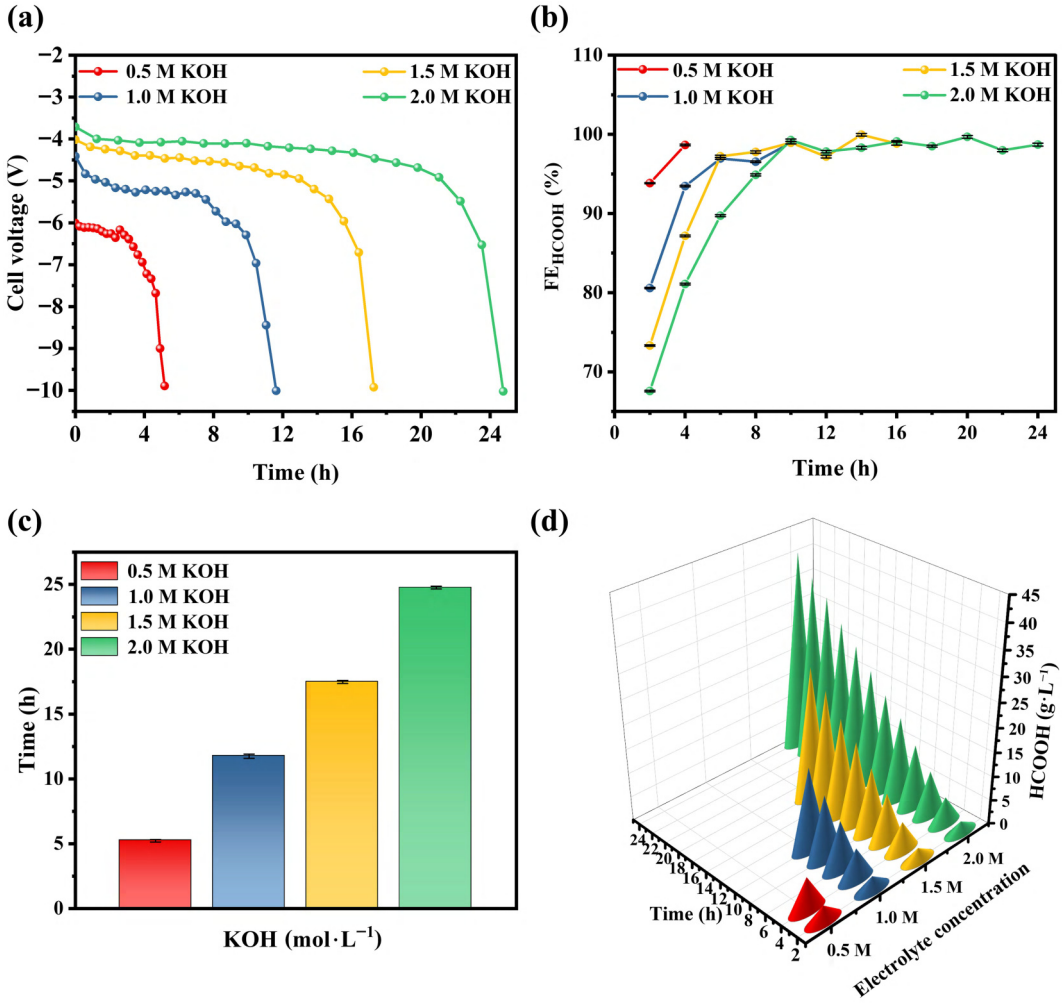


Figure 4 Effects of KOH electrolyte concentration. (a) Variation of cell voltage over time at different KOH concentrations. (b) Influence of KOH concentration on the FE for formate. (c) Time required to reach −10 V during electrolysis at various KOH concentrations. (d) Effect of KOH concentration on formate production.

direction of the cell's electromotive force (Fig. 5(a)). In theory, this approach can effectively offset part of the cell voltage increase caused by the reverse diffusion of K^+, thereby addressing the issue of continuously rising cell voltage during formate accumulation.

Experiments were first carried out using $KHCO_3$ as the electrolyte. As shown in Fig. 5(b), the initial cell voltage was approximately −6 V, and as the reaction proceeded, the voltage curve exhibited an arch-shaped trend of "first decreasing and then increasing". This change originated from a reverse diffusion potential generated by the initial concentration difference between the anode and cathode, which effectively offset part of the ohmic voltage drop. During this stage, K^+ migrated along the concentration gradient, and when the K^+ concentrations in the cathode and anode chambers became similar, the cell voltage reached its minimum. Subsequently, K^+ began to migrate against the concentration gradient, and the cell voltage gradually increased. Overall, this strategy was able to maintain cell voltage fluctuations within ±0.5 V for up to 30 h, and the accumulated formate concentration reached approximately 50.6 mg·L^{-1}. As shown in Fig. 5(c), most current studies use the same electrolyte concentration in both the anode and cathode chambers, and to increase formate concentration, they typically replace only the anolyte with fresh solution when the cell voltage nearly doubles. In this work, the anolyte was refreshed each time the cell voltage increased by −1 V. After seven anolyte refreshments, a sample was taken at the 50th hour of the reaction, and the accumulated formate concentration was found to reach 73.3 mg·L^{-1}, while the FE dropped to 85.18%. As shown in Fig. 5(d), the method of simultaneously refreshing both the catholyte and anolyte requires frequent renewal of the catholyte, making it difficult to accumulate high concentrations of the product. Therefore, this method is only suitable for catalyst performance evaluation and will not be discussed in detail here.

Subsequently, the same experiment was conducted using KOH as the electrolyte. As shown in Fig. 5(e), similarly, the cell voltage exhibited a "first decreasing and then increasing" trend as the reaction progressed, forming an arch-shaped curve. Compared with the $KHCO_3$ system, the duration of voltage fluctuation within the range of ±0.5 V in the KOH system lasted for approximately 33 h, slightly longer than that in the $KHCO_3$ system, and the formate concentration accumulated in a single run reached approximately 55.4 mg·L^{-1}. As shown in Fig. 5(f), after five anolyte refreshments, a sample was taken at the 52nd hour, and the formate concentration reached 78.8 mg·L^{-1}, with the FE dropping to 88.29%. It is also worth noting that in the KOH system, the interval between each anolyte replacement was about 2 h longer than that in the $KHCO_3$ system, indicating a better capability in maintaining a low cell voltage. As shown in Fig. 5(g), the result of simultaneously

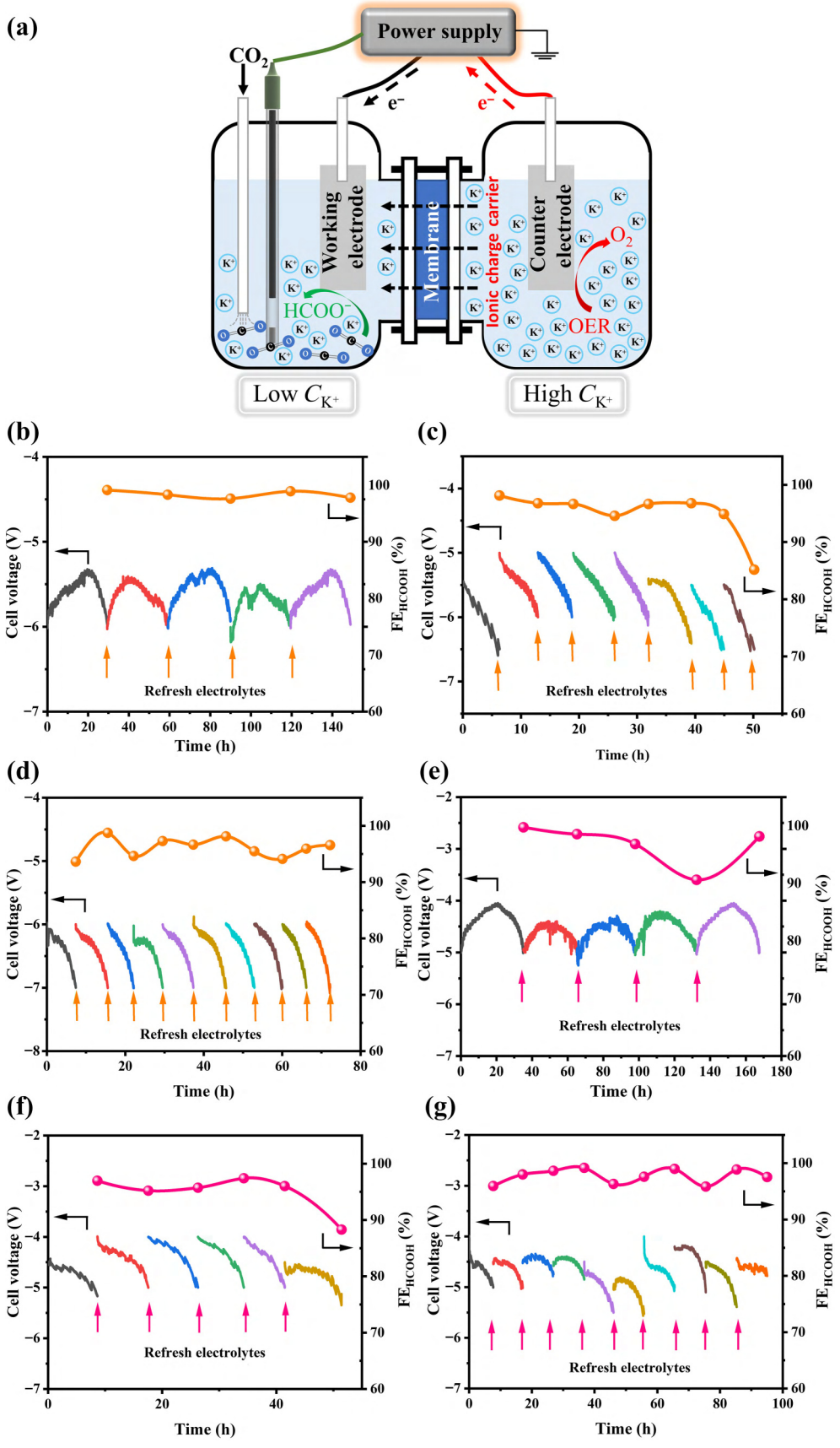


Figure 5 Cell voltage and FE for formate production under different strategies. (a) Schematic diagram of the concentration-gradient strategy. ((b)–(d)) Using $KHCO_3$ electrolyte: (b) concentration-gradient strategy, (c) replacing anolyte only, and (d) replacing both catholyte and anolyte. ((e)–(g)) Using KOH electrolyte: (e) concentration-gradient strategy, (f) replacing anolyte only, and (g) replacing both catholyte and anolyte.

refreshing both the catholyte and anolyte (KOH) was similar to that the $KHCO_3$ system, and thus is not discussed in detail here.

In summary, the "concentration-gradient" strategy enables the cell voltage to be maintained within ±0.5 V for over 30 h, which is 3–4 times longer than the current average level (Table S1 in the ESM). The formate production rate reached 310 μmol·cm^{-2}·h^{-1}·mA^{-1}, approximately 200% of the current average level (Table S2 in the ESM). In this work, K^+ was used as the primary charge carrier, which essentially represents the case of cation-based charge transport. To verify the universality of the "concentration-gradient" strategy, $NaHCO_3$ was used as the electrolyte, and the strategy was still effective (Figs. S8 and S9 in the ESM). This indicates that as long as cations act as the charge carriers, this strategy can effectively address the issue of continuously increasing cell voltage during long-term formate accumulation. In the future, regardless of the specific CO_2RR product, this strategy holds feasibility and application potential.

4 Conclusions

In summary, this study systematically investigated the electrolyte evolution mechanism and its influence on cell voltage during the electrocatalytic reduction of CO_2 to formate in the mainstream H-type cell system, which employs neutral/alkaline electrolytes combined with a cation exchange membrane. Dynamic monitoring of ion concentrations, conductivity, and pH in both chambers revealed that the continuous migration of K^+, the main charge carrier, is the primary cause of the gradual voltage increase. Based on this insight, a concentration-gradient strategy was proposed and validated, using a saturated electrolyte (3.37 mol·L^{-1}) anolyte and a low-concentration (0.5 mol·L^{-1}) catholyte to generate a reverse diffusion potential. This strategy effectively offsets the Ohmic drop, enabling the electrocatalytic reduction of CO_2 to formate under a controllable cell voltage with efficient formate accumulation.

Electronic Supplementary Material: Supplementary material (experimental characterizations, electrochemical test data, comparative tables, and Figs. S1–S9) is available in the online version of this article at https://doi.org/10.26599/NR.2026.94908710.

Data availability

All data needed to support the conclusions in the paper are presented in the manuscript and the Electronic Supplementary Material. Additional data related to this paper may be requested from the corresponding author upon request.

Acknowledgements

This work was supported by the National Natural Science Foundation of China (Nos. 52474319, 52450003, 52250091, and U2341267), the National Science Fund for Distinguished Young Scholars (No. 52025041), and the Fundamental Research Funds for the Central Universities of (No. FRF-TP-20-02C2). Furthermore, this project were supported by the Interdisciplinary Research Project for Young Teachers of USTB (Fundamental Research Funds for the Central Universities) (No. FRF-IDRY-GD23-003), Beijing Key Laboratory of High-Entropy Energy materials and Devices, Beijing Institute of Nanoenergy and Nanosystems (No. GS2025MS022), and Key Laboratory of Green Extraction & Efficient Utilization of Light Rare-Earth Resources (Inner Mongolia University of Science and Technology), Ministry of Education (No. REKF26004).

Declaration of competing interest

All the contributing authors report no conflict of interests in this work.

Author contribution statement

J. H. L.: Writing – original draft. L. M. Y.: Investigation. T. Y.: Writing – review & editing, supervision, funding acquisition. S. B. D.: Investigation. S. L.: Methodology. K. W.: Data curation. X. T. Y.: Data curation. S. C.: Resources. Z. T. D.: Methodology. S. L. L.: Methodology. X. M. H.: Funding acquisition, project administration. All the authors have approved the final manuscript.

Use of AI statement

None.

References

[1] García De Arquer, F. P.; Dinh, C. T.; Ozden, A.; Wicks, J.; McCallum, C.; Kirmani, A. R.; Nam, D. H.; Gabardo, C.; Seifitokaldani, A.; Wang, X. et al. CO_2 electrolysis to multicarbon products at activities greater than 1 A·cm^{-2}. *Science* **2020**, *367*, 661–666.

[2] Xia, C.; Zhu, P.; Jiang, Q.; Pan, Y.; Liang, W. T.; Stavitski, E.; Alshareef, H. N.; Wang, H. T. Continuous production of pure liquid fuel solutions via electrocatalytic CO_2 reduction using solid-electrolyte devices. *Nat. Energy* **2019**, *4*, 776–785.

[3] Gu, J.; Liu, S.; Ni, W. Y.; Ren, W. H.; Haussener, S.; Hu, X. L. Modulating electric field distribution by alkali cations for CO_2 electroreduction in strongly acidic medium. *Nat. Catal.* **2022**, *5*, 268–276.

[4] Chen, T.; Hu, Q. Z.; Wu, C.; Sun, M. D.; Fu, P.; Liu, X. L.; Li, Y. L.; Zhou, Y.; Xi, S. B.; Wang, J. Ultralow-coordinated Ni species boosting paired electrosynthesis of formate from waste plastic and carbon dioxide. *J. Energy Chem.* **2025**, *107*, 285–295.

[5] Cai, M.; Zhang, P. P.; Yang, J.; Han, M. X.; Huang, J. R.; Xiao, H. Y.; Han, J. B.; Zhang, X. Y.; Jiang, H. C. Salinity and nutrient availability dictate methane production and its temperature sensitivity in lakes. *Water Res.* **2026**, *289*, 124836.

[6] Ferrer, M.; Pham, A. N.; Waite, T. D. Optimising pollutant degradation in reductant-mediated copper Fenton-like systems using mechanistically-based kinetic modelling. *Water Res.* **2025**, *287*, 124339.

[7] Ul, Z.; Sulonen, M.; Haus, P.; Izadi, P.; Baeza, J. A.; Harnisch, F.; Guisasola, A. Evaluation of single chamber electrochemical reduction of CO_2 to formate for application under biocompatible conditions. *J. CO_2 Util.* **2025**, *97*, 103136.

[8] Zeng, J. Q.; Castellino, M.; Fontana, M.; Sacco, A.; Monti, N. B. D.; Chiodoni, A.; Pirri, C. F. Electrochemical reduction of CO_2 with good efficiency on a nanostructured Cu-Al catalyst. *Front. Chem.* **2022**, *10*, 931767.

[9] Wen, G. B.; Lee, D. U.; Ren, B. H.; Hassan, F. M.; Jiang, G. P.; Cano, Z. P.; Gostick, J.; Croiset, E.; Bai, Z. Y.; Yang, L. et al. Orbital interactions in Bi-Sn bimetallic electrocatalysts for highly selective electrochemical CO_2 reduction toward formate production. *Adv. Energy Mater.* **2018**, *8*, 1802427.

[10] Ma, W. C.; Xie, S. J.; Zhang, X. G.; Sun, F. F.; Kang, J. C.; Jiang, Z.; Zhang, Q. H.; Wu, D. Y.; Wang, Y. Promoting electrocatalytic CO_2 reduction to formate via sulfur-boosting water activation on indium surfaces. *Nat. Commun.* **2019**, *10*, 892.

[11] Fan, M. Y.; Prabhudev, S.; Garbarino, S.; Qiao, J. L.; Botton, G. A.; Harrington, D. A.; Tavares, A. C.; Guay, D. Uncovering the nature of electroactive sites in nano architectured dendritic Bi for highly efficient CO_2 electroreduction to formate. *Appl. Catal. B: Environ.* **2020**, *274*, 119031.

[12] Izadi, P.; Kas, A.; Haus, P.; Harnisch, F. On the stability of electrochemical CO_2 reduction reaction to formate at indium electrodes at biocompatible conditions. *Electrochim. Acta* **2023**, *462*, 142733.

[13] Cui, X. L.; Wu, M.; Hou, G. Y.; Li, Y. C.; Wang, Y. N.; Wang, Y. A.; Huang, J. J.; Zhao, M.; Luo, Z. Z.; Zou, Z. G. et al. Alkali metal ions stabilizing copper(I)-sulfur bonds for efficient formate production from electrochemical CO_2 reduction. *ACS Catal.* **2024**, *14*, 11857–11864.

[14] Chi, L. P.; Niu, Z. Z.; Zhang, X. L.; Yang, P. P.; Liao, J.; Gao, F. Y.; Wu, Z. Z.; Tang, K. B.; Gao, M. R. Stabilizing indium sulfide for CO_2 electroreduction to formate at high rate by zinc incorporation. *Nat. Commun.* **2021**, *12*, 5835.

[15] Li, Y. C.; Delmo, E. P.; Hou, G. Y.; Cui, X. L.; Zhao, M.; Tian, Z. H.; Zhang, Y.; Shao, M. Enhancing local CO_2 adsorption by L-histidine incorporation for selective formate production over the wide potential window. *Angew. Chem.* **2023**, *135*, e202313522.

[16] Liang, X. D.; Zheng, Q. Z.; Wei, N.; Lou, Y. Y.; Hu, S. N.; Zhao, K. M.; Liao, H. G.; Tian, N.; Zhou, Z. Y.; Sun, S. G. *In-situ* constructing $Bi@Bi_2O_2CO_3$ nanosheet catalyst for ampere-level CO_2 electroreduction to formate. *Nano Energy* **2023**, *114*, 108638.

[17] Lei, P. X.; Liu, S. Q.; Wen, Q. R.; Wu, J. Y.; Wu, S.W.; Wei, X. X.; Feng, R. F.; Fu, X. Z.; Luo, J. L. Integrated "two-in-one" strategy for high-rate electrocatalytic CO_2 reduction to formate. *Angew. Chem., Int. Ed.* **2025**, *64*, e202415726.

[18] Yi, L. C.; Chen, J. X.; Shao, P.; Huang, J. H.; Peng, X. X.; Li, J. W.; Wang, G. X.; Zhang, C.; Wen, Z. H. Molten-salt-assisted synthesis of bismuth nanosheets for long-term continuous electrocatalytic conversion of CO_2 to formate. *Angew. Chem., Int. Ed.* **2020**, *59*, 20112–20119.

[19] Li, Z. Y.; Wang, P.; Han, G. Q.; Yang, S. Z.; Roy, S.; Xiang, S. T.; Jimenez, J. D.; Kondapalli, V. K. R.; Lyu, X.; Li, J. L. et al. Ampere-level co-electrosynthesis of formate from CO2 reduction paired with formaldehyde dehydrogenation reactions. *Nat. Commun.* **2025**, *16*, 4850.

[20] Kang, Y.; Kim, T.; Jung, K. Y.; Park, K. T. Recent progress in electrocatalytic CO_2 reduction to pure formic acid using a solid-state electrolyte device. *Catalysts* **2023**, *13*, 955.

[21] Fernández-Caso, K.; Díaz-Sainz, G.; Alvarez-Guerra, M.; Irabien A. Electroreduction of CO_2: Advances in the continuous production of formic acid and formate. *ACS Energy Lett.* **2023**, *8*, 1992–2024.

[22] Ibanez, R.; Stamatialis, D. F.; Wessling, M. Role of membrane surface in concentration polarization at cation exchange membranes. *J. Membr. Sci.* **2004**, *239*, 119–128.

[23] Zheng, Z.; Yao, Y. F.; Yan, W.; Bu, H. Y.; Huang, J. F.; Ma M. Mechanistic insights into the abrupt change of electrolyte in CO_2 electroreduction. *ACS Catal.* **2024**, *14*, 6328–6338.

[24] Nankya, R.; Xu, Y. T.; Elgazzar, A.; Zhu, P.; Wi, T. U.; Qiu, C.; Feng, Y. G.; Che, F. L.; Wang, H. T. Cobalt-doped bismuth nanosheet catalyst for enhanced electrochemical CO_2 reduction to electrolyte-free formic acid. *Angew. Chem.* **2024**, *136*, e202403671.

[25] Shen, H. D.; Zhao, Y. K.; Zhang, L.; He, Y.; Yang, S. W.; Wang, T. S.; Cao, Y. L.; Guo, Y.; Zhang, Q. Y.; Zhang, H. P. *In-situ* constructuring of copper-doped bismuth catalyst for highly efficient CO_2 electrolysis to formate in ampere-level. *Adv. Energy Mater.* **2023**, *13*, 2202818.

[26] Li, W. B.; Yu, C.; Tan, X. Y.; Ren, Y. W.; Zhang, Y. F.; Cui, S.; Yang, Y.; Qiu, J. S. Beyond leverage in activity and stability toward CO_2 electroreduction to formate over a bismuth catalyst. *ACS Catal.* **2024**, *14*, 8050–8061.

[27] Liang, S. Y.; Xiao, J. W.; Zhang, T. Y.; Zheng, Y.; Wang, Q.; Liu B. Sulfur changes the electrochemical CO_2 reduction pathway over Cu electrocatalysts. *Angew. Chem.* **2023**, *135*, e202310740.

[28] Wang, Z. T.; Qi, R. J.; Liu, D. Y.; Zhao, X. D.; Huang, L.; Chen, S. H.; Chen, Z. Q.; Li, M. T.; You, B.; Pang, Y. J. et al. Exfoliated ultrathin $ZnIn_2S_4$ nanosheets with abundant zinc vacancies for enhanced CO_2 electroreduction to formate. *ChemSusChem.* **2021**, *14*, 852–859.

[29] Liu, J. Z.; Li, Y. H.; Wang, Y. T.; Xiao, C. Q.; Liu, M. M.; Zhou, X. D.; Jiang, H.; Li, C. Z. Isolated ultrasmall Bi nanosheets for efficient CO_2-to-formate electroreduction. *Nano Res.* **2022**, *15*, 1409–1414.

[30] Li, Z. Y.; Yang, Y. S.; Ding, H.; Li, Z.; Wang, L.; Zhang, X.; Li, J.; Xie, W. F.; Hu, X. Y.; Wang, B. et al. *In situ* investigations on Bi-based electrocatalyst construction and reaction dynamic monitoring toward efficient CO_2 reduction. *Chem. Catal.* **2023**, *3*, 100767.

[31] Xie, H. X.; Lv, L.; Sun, Y.; Wang, C. L.; Xu, J. L.; Tang, M. CuSnBi catalyst grown on copper foam by Co-electrodeposition for efficient electrochemical reduction of CO_2 to formate. *Catalysts.* **2024**, *14*, 191.

[32] Peng, L. W.; Chen, C. S.; He, R. N.; Xu, N. N.; Qiao, J. L.; Lin, Z. Z.; Zhu, Y.; Huang, H. T. Tin-doped bismuth dendrites for highly efficient electrocatalytic reduction of CO_2 by using bipolar membrane in ultrathin liquid reactor. *EcoMat* **2022**, *4*, e12260.

[33] Sui, P. F.; Xu, C. Y.; Zhu, M. N.; Liu, S. B.; Liu, Q. X.; Luo, J. L. Interface-induced electrocatalytic enhancement of CO_2-to-formate conversion on heterostructured bismuth-based catalysts. *Small* **2022**, *18*, e2105682.

[34] Zeng, G.; He, Y. C.; Ma, D. D.; Luo, S. W.; Zhou, S. H.; Cao, C. S.; Li, X. F.; Wu, X. T.; Liao, H. G.; Zhu, Q. L. Reconstruction of ultrahigh-aspect-ratio crystalline bismuth-organic hybrid nanobelts for selective electrocatalytic CO_2 reduction to formate. *Adv. Funct. Mater.* **2022**, *32*, 2201125.

[35] Wang, Y. C.; Sui, P. F.; Xu, C. Y.; Zhu, M. N.; Feng, R. F.; Ma, H. T.; Zeng, H. B. Optimizing Bi active sites by Ce doping for boosting formate production in a wide potential window. *Inorg. Chem. Front.* **2024**, *11*, 926–935.

[36] Li, S. H.; Hu, S. Q.; Liu, H. M.; Liu, J. R.; Kang, X.; Ge, S. Y.; Zhang, Z. Y.; Yu, Q. M.; Liu, B. L. Two-dimensional metal coordination polymer derived indium nanosheet for efficient carbon dioxide reduction to formate. *ACS Nano.* **2023**, *17*, 9338–9346.

[37] Zhang, M.; Wei, W. B.; Zhou, S. H.; Ma, D. D.; Cao, A. H.; Wu, X. T.; Zhu, Q. L. Engineering a conductive network of atomically thin bismuthene with rich defects enables CO_2 reduction to formate with industry-compatible current densities and stability. *Energy Environ. Sci.* **2021**, *14*, 4998–5008.

[38] Chen, Y. X.; Choi, J.; Liang, F. K.; Tan, X. Y.; Chen, Y. D.; Yang, J. H.; Hong, S.; Zhang, X.; Robertson, A. W.; Jung, Y. et al. Synergistic catalysis between In single atoms and In nanoparticles for highly selective electrocatalytic CO_2 reduction to formate with high current densities. *Chem. Sci.* **2025**, *16*, 11574–11580.

[39] Liu, S. T.; Tian, B. L.; Xu, X. R.; Wang, X. Z.; Ran, P.; Sun, Y. M.; Wu, J. H.; Qiu, A. Q.; Wang, F. Y.; Tang, L. Y. et al. Ampere-level electrolytic coproduction of formate with coupled carbon dioxide reduction and selective methanol oxidation. *ACS Catal.* **2024**, *14*, 9476–9486.

[40] Sui, P. F.; Gao, M. R.; Liu, S. B.; Xu, C. Y.; Zhu, M. N.; Luo, J. L. Carbon dioxide valorization via formate electrosynthesis in a wide potential window. *Adv. Funct. Mater.* **2022**, *32*, 2203794.

[41] Wei, Z. M.; Ding, J.; Wang, Z. Y.; Wang, A. Y.; Zhang, L.; Liu, Y. H.; Guo, Y. Z.; Yang, X.; Zhai, Y. M.; Liu, B. Enhanced electrochemical CO_2 reduction to formate over phosphate-modified in: Water activation and active site tuning. *Angew. Chem., Int. Ed.* **2024**, *63*, e202402070.

[42] Teng, X.; Shi, K.; Chen, L. S.; Shi, J. L. Coupling electrochemical sulfion oxidation with CO_2 reduction over highly dispersed p-Bi nanosheets and CO_2-assisted sulfur extraction. *Angew. Chem.* **2024**, *136*, e202318585.

[43] Ren, X. X.; Liu, F.; Wu, H.; Lu, Q.; Zhao, J.; Liu, Y.; Zhang, J. F.;

Mao, J.; Wang, J. J.; Han, X. P. et al. Reconstructed bismuth oxide through *in situ* carbonation by carbonate-containing electrolyte for highly active electrocatalytic CO_2 reduction to formate. *Angew. Chem., Int. Ed.* **2024**, *63*, e202316640.

[44] Mališ, J.; Mazúr, P.; Paidar, M.; Bystron, T.; Bouzek, K. Nafion 117 stability under conditions of PEM water electrolysis at elevated temperature and pressure. *Int. J. Hydrogen Energy* **2016**, *41*, 2177–2188.

[45] Qiao, Y.; Lai, W. C.; Huang, K.; Yu, T. T.; Wang, Q. Y.; Gao, L.; Yang, Z. L.; Ma, Z. S.; Sun, T. L.; Liu, M. et al. Engineering the local microenvironment over Bi nanosheets for highly selective electrocatalytic conversion of CO_2 to HCOOH in strong acid. *ACS Catal.* **2022**, *12*, 2357–2364.

[46] Yang, S.; An, H. Y.; Arnouts, S.; Wang, H.; Yu, X.; De Ruiter, J.; Bals, S.; Altantzis, T.; Weckhuysen, B. M.; Van Der Stam, W. Halide-guided active site exposure in bismuth electrocatalysts for selective CO_2 conversion into formic acid. *Nat. Catal.* **2023**, *6*, 796–806.

[47] Xu, B. Q.; Masood Ul Hasan, I.; Peng, L. W.; Liu, J. Y.; Xu, N. N.; Fan, M. Y.; Niazi, N. K.; Qiao, J. L. Anion-regulation engineering toward Cu/In/MOF bimetallic electrocatalysts for selective electrochemical reduction of CO_2 to CO/formate. *Mater. Rep.: Energy* **2022**, *2*, 100139.

[48] Ma, M.; Clark, E. L.; Therkildsen, K. T.; Dalsgaard, S.; Chorkendorff, I.; Seger, B. Insights into the carbon balance for CO_2 electroreduction on Cu using gas diffusion electrode reactor designs. *Energy Environ. Sci.* **2020**, *13*, 977–985.

[49] Liu, J. H.; Yang, T.; Yang, L. M.; Huang, G. C.; Wang, E. H.; Wang, K.; Wang, H. Y.; Hou, X. M. Stability enhancement strategy for LOM-based oxygen evolution reaction catalyst. *Surf. Interfaces* **2025**, *72*, 107169.

[50] Guo, M. W.; Zhang, Z.; Zhang, H. R.; Lin, J. J.; Qin, X. S.; Deng, R. R.; Gao, M. Y.; Zhang, Q. B. Dual-phase spinel manganese-cobalt hybrid oxide for enhanced oxygen evolution catalysis in acid media. *J. Energy Chem.* **2025**, *108*, 361–372.

[51] Liu, X.; Monteiro, M. C. O.; Koper, M. T. M. Interfacial pH measurements during CO_2 reduction on gold using a rotating ring-disk electrode. *Phys. Chem. Chem. Phys.* **2023**, *25*, 2897–2906.

[52] Monteiro, M. C. O.; Philips, M. F.; Schouten, K. J. P.; Koper, M. T. M. Efficiency and selectivity of CO_2 reduction to CO on gold gas diffusion electrodes in acidic media. *Nat. Commun.* **2021**, *12*, 4943.

[53] Petrov, K. V.; Koopman, C. I.; Subramanian, S.; Koper, M. T. M.; Burdyny, T.; Vermaas, D. A. Bipolar membranes for intrinsically stable and scalable CO_2 electrolysis. *Nat. Energy* **2024**, *9*, 932–938.

[54] Lee, C. W.; Cho, N. H.; Im, S. W.; Jee, M. S.; Hwang, Y. J.; Min, B. K.; Nam, K. T. New challenges of electrokinetic studies in investigating the reaction mechanism of electrochemical CO_2 reduction. *J. Mater. Chem. A* **2018**, *6*, 14043–14057.

This is an open access article under the terms of the Creative Commons Attribution 4.0 International License (CC BY 4.0, https://creativecommons.org/licenses/by/4.0/).

© The Author(s) 2026. Published by Tsinghua University Press.